Impact of synthesis method on the properties of near-infrared region-reflective $SrSn_{0.9}Mn_{0.1}O_3$ brown pigment

J. Hroch*, Ž. Dohnalová, P. Šulcová

Department of Inorganic Technology, Faculty of Chemical Technology, University of Pardubice,

Studentská 95, 53210 Pardubice, Czech Republic

**e-mail: jan.hroch@upce.cz*

Abstract

Brown near-infrared region (NIR) reflective pigment of $SrSn_{0.9}Mn_{0.1}O_3$ was prepared using four different methods: the classical ceramic method, both wet and dry mechanochemical activation processes and the precipitation method. The pigments were characterised in terms of colour properties, NIR reflectivity, phase composition, particle size distribution and particle morphology. The prepared powders were applied to the organic matrix in mass tone, and their resulting colour hues shifted from copper brown via chocolate brown to dark brown. The NIR solar reflectance was calculated in the wavelength interval of 700–1,650 nm following the ASTM 173-03 standard and their values of powder form were 25% – 44%. The colour hue and NIR solar reflectance were dependent on the calcination temperature and the preparation method. The optimal condition for the preparation of the most NIR-reflective saturated brown pigment is the precipitation method and a temperature of 1,050°C (R_{solar} = 42%; $C_{powder\ form}$ = 18.4), with an interesting matchstick shape of particles.

Keywords: A. Powders: solid-state reaction; C. Colour; D. Perovskites; cool pigments

1 Introduction

In recent years, ABO_3 perovskite compounds have received considerable attention due to their optical, catalytic, magnetic and electrical properties [1,2,3,4,5]. Special interest has been focused on the development of these materials, which are adjusted by rare earth elements or transition metals [6] to form interesting multifunctional products, such as solar cells [7,8], transparent electrodes in LEDs [9], lasers [10] and photodetectors [11,12]. The important group of perovskites are alkaline earth stannates, which include $CaSnO_3$, $SrSnO_3$ and $BaSnO_3$ with interesting dielectric, electronic and gas-sensing properties [6,13,14], which could be applied in the production of humidity [15], gas sensors [16], capacitor components, and other applications [17,18]. These compounds have a wide band gap ($CaSnO_3$: 4.4 eV; $SrSnO_3$: 4.1 eV, $BaSnO_3$: 3.3 eV) [19,20], which is caused by a large space between the valence band of O 2p orbitals and the conduction band of the Sn 5s orbitals [20].

Among the stannates, the strontium stannate has the same orthorhombic structure as $GdFeO_3$ [20], with a symmetry group of Pbnm, while its lattice parameters are a = 0.5703 nm, b = 0.8065 nm and c = 0.5708 nm [21]. The high value of the band gap causes the basic structure to exhibit a white colour, since it can only absorb light in the ultraviolet region [22]. One of the effective means for improving and allowing the $SrSnO_3$ to absorb a wider wavelength interval, mainly the wavelength in the visible region, involves incorporating the dopant into the structure [23]. According to the literature, compounds doped with cations of $Tb^{3+,4+}$ and Mo^{6+} of strontium stannate compounds have been widely explored and tested as a dark green pigment, described as a cubic structure with the lattice parameter a = 0.4089 nm [24]. Due to the use of a Tb dopant only, the strontium stannate exhibited to drop a wide band gap from 4.1 eV to 2.65 eV, leading to the absorption of a part of visible light and the formation of new yellow pigments [24,25]. Elsewhere, $SrSnO_3$ compounds doped with V^{5+} were studied in terms of pigmentary properties and provided yellow hues of efficient yellow colour hues in ceramic glaze [26]. In an earlier report, it was found that the doping of Cr in $SrSnO_3$ led to enhanced pigment properties, mainly in the field of near-infrared region (NIR) reflectivity, and these were marked as cool pigments [27]. These pigments are characterised by high solar reflectance in the NIR, and not only play a significant role in the reduction of surfaces and the indoor temperature of buildings but also in reducing the consumption of electric energy in the summer season [28,29].

Sunlight consists of a 5% ultraviolet spectrum (280–400 nm), a 43% visible spectrum (400–700 nm) and 52% near-infrared spectrum (700–2,500 nm) [30], where the wavelength interval of 700–1,300 nm corresponds approximately to 80% of the total heat energy in the NIR range [31]. For this reason, it is important to shield NIR radiation using the previously mentioned cool pigments. While NIR pigments have been studied along with their potential applications [27,30,32,33,34,35], there is limited information about $SrSnO_3$ as a cool pigment.

This paper deals with a doped strontium stannate brown pigment with a low manganese content ($SrSn_{0.9}Mn_{0.1}O_3$) that could replace commercially produced brown pigments containing of Cr^{3+} (the production of which involves dichromate). The perovskite was synthesised by classical ceramic method (CCM), dry mechanochemical activation (DMA), and wet mechanochemical activation (WMA), and precipitation method (PM). The effect of the preparation method on the pigmentary application properties and their pre-application testing of reflectance in the NIR range is then evaluated. Moreover, the phase

purity and morphological characteristics of the prepared powders are also analysed via X-ray diffraction analysis and scanning electron microscopy.

2 Materials and methods

2.1 Preparation methods

The perovskite pigment of $SrSn_{0.9}Mn_{0.1}O_3$ was prepared using four different preparation approaches. The first three methods of preparation are based on a solid-state reaction. For the preparation of the samples in this manner, a stoichiometric amount of SnO_2 (99%, Shepherd Color Company, USA), $SrCO_3$ (99.9%, Sigma-Aldrich, Italy) and MnO_2 (99%, Lachema Brno, Czech Republic) were used as starting compounds. The first procedure was the classical ceramic method (CCM). Here, the starting materials were mixed in a ceramic mortar and then calcined at temperatures of 1,050°C, 1,200°C, 1,300°C and 1,400°C for four hours, with a heating rate of 10°C/min [36]. The formation of pigment is described by Equation (1):

$$SrCO_3 + 0.9\ SnO_2 + 0.1\ MnO_2 \rightarrow SrSn_{0.9}Mn_{0.1}O_3 + CO_2 \quad (1)$$

In the second method, the CCM was supplemented by the dry mechanochemical process (DMA). Initial mixtures were activated in the planetary mill (Fritsch Pulverisette 5). The milling conditions followed a rotation velocity of 200 rpm, a grinding time of five hours and agate balls (Ø 2 cm) in a powder mass ratio of 10:1. The resulting activated mixture was heated under the same conditions as in the CCM procedure [36].

The mechanochemical process was also carried out in a wet medium of ethanol (WMA). The milling process was performed as in the case of the DMA. The mixture obtained was dried in an electric dryer at a temperature of 70°C. The dried mixture was exposed to the same calcination process as in the previous methods.

For the precipitation method (PM), $Na_2SnO_3 \cdot 3H_2O$ (95%, Sigma-Aldrich, USA), $Sr(NO_3)_2$ (99.9%, Sigma-Aldrich, India) and $Mn(NO_3)_2 \cdot 4H_2O$ (99.5%, Lach-Ner, Czech Republic) were used as initial reagents. First, the powder of $Sr(NO_3)_2$ was dissolved in 400 ml of distilled water and then stirred. In the second step, $Mn(NO_3)_2 \cdot 4H_2O$ was dissolved in a solution of $Sr(NO_3)_2$ and stirred intensively. The NaOH solution was then dropped into the nitrate solution and the pH of the solution was adjusted to 10. Following this, the $Na_2SnO_3 \cdot 3H_2O$ was dissolved in 300 ml of distilled water and then slowly added to the nitrate solution. The above-mixed solution was then stirred for 10 minutes to obtain a brown precipitate of $SrSn_{0.9}Mn_{0.1}(OH)_6$.

Finally, the precipitate was filtered, washed in 800 ml of distilled water and dried in an electric dryer at a temperature of 80°C [37]. The dried precursor was then ground and calcined at a temperature of 800°C, 950°C and 1,050°C for four hours with a growth temperature rate of 10°C/min. The formation of pigments is described by Equation (2):

$$0.1\ Mn(NO_3)_2 + Sr(NO_3)_2 + 0.9\ Na_2SnO_3 + 0.05\ O_2 + 0.4\ NaOH \rightarrow SrSn_{0.9}Mn_{0.1}O_3 + 2.2\ NaNO_3 + 0.2\ H_2O \quad (2)$$

The prepared samples were milled using a planetary mill (Fritsch Pulverisette 5). The milling process was carried out in an agate bowl with zircon balls (SiLibeads Ø 1.6–1.8 mm), with a spinning rate of 200 rpm for 10 minutes. The ball-to-powder weight ratio was 8:1 in the ethanol medium. The milled powders were characterised using several techniques.

2.2 Characterisation techniques

For the identification of the phase composition, the powder X-ray diffraction pattern of the prepared pigment was recorded using a diffractometer (Rigaku MiniFlex 600). The device was equipped with a Cu anode (radiation $K_\alpha \lambda$ = 0.15418 nm) and a semiconductor detector D/TEX Ultra High Speed 1D. Data were collected via step scanning in a 2θ range from 10° to 80°, with a step size of 0.02° and a scanning speed of 10°/min. The diffraction patterns were evaluated with reference to the PDF2 database [36].

The relevant equipment (Malvern Mastersizer 2000/MU) was used to measure the particle size distribution, with the resulting signals evaluated based on the Mie theory. Prior to the measurement, the samples were dispersed in a solution of $Na_2P_4O_7$. The particle size distribution is expressed by values of d_{50} and the width of the distribution (SPAN). The SPAN was obtained using Equation (3) [38]:

$$SPAN = \frac{d_{90} - d_{10}}{d_{50}} \quad (3)$$

The microstructure characterisation of the powders was studied using a scanning electron microscope (Tescan Lyra 3) with an accelerating voltage of 10 kV. Powders for microanalysis determinations were deposited in a carbon holder and sputtered with gold.

The diffuse reflectance of the powdered pigments in the wavelength range of 700–1,650 nm was measured with a spectrophotometer (Shimadzu UV-3600 Plus) using barium sulphate as the reflectance standard. The apparatus was equipped with a white ISR-603 integration sphere attachment and a semiconductor detector

of InGaAs. The measured data were used to compute the solar reflectance *R** according to the ASTM G173-03 standard. This parameter could be derived using Equation (4):

$$R^* = \frac{\int_{700}^{1650} r(\lambda) \cdot i(\lambda) \cdot d\lambda}{\int_{700}^{1650} i(\lambda) \cdot d\lambda} \quad (4)$$

where *r(λ)* is the reflectance obtained experimentally [%] and *i(λ)* is the standard solar spectral irradiance [$W \cdot m^{-2} \cdot nm^{-1}$], as obtained with reference to the ASTM standard [27,39].

The optical properties of the samples and their applications into an organic binder in mass tone were analysed using a spectrophotometer (HunterLab UltraScan VIS). The measurement conditions were as follows: standard illuminant D65, 10° complementary observant and measurement geometry d/8°. The colour characteristics were described as per the CIE *L*a*b** system (1976), where *L** represents lightness or darkness and moves from 0 (black) to 100 (white). The colour coordinates *a** and *b** indicate the following colour hues: *a** (red-green) and *b** (yellow-blue). For a better description of the colour, the chroma (C) represents a saturation of the colour and is calculated according to Equation (5) [40]:

$$C = \sqrt{a^{*2} + b^{*2}} \quad (5)$$

3 Results and discussion

3.1 Powder X-ray diffraction analysis

The phase composition of $SrSn_{0.9}Mn_{0.1}O_3$ was examined via powder X-ray diffraction (XRD) analysis. The phases identified in the calcined samples at different temperatures and prepared using the different methods are shown in Table 1. It is clear that the powders prepared via solid-state reactions (CCM, DMA and WMA) provide a one-phase compound at high temperatures. The samples prepared via the CCM and WMA methods with a calcining temperature of 1,050°C contained nonreacted starting materials of SnO_2 (PDF No. 00-021-1250), the spinel phase of Sr_2SnO_4 (PDF No. 01-089-037) and the perovskite phase of $SrSnO_3$ (PDF No. 01-081-2514). A similar multiphase product was also identified when using the DMA method, but the identified phases are termed the perovskite phase of $SrSnO_3$ and $SrMnO_3$ (PDF No. 01-072-019), an unreacted SnO_2. The single-phase powder corresponding to the perovskite phase of $SrSnO_3$ was found at a temperature of 1,200°C in the samples prepared via the CCM and DMA methods, while the sample prepared via the WMA method did not provide a single-phase product, with this sample consisting of $SrSnO_3$ and a small amount of SnO_2. At 1,300°C, all the raw materials were completely reacted across all

the processes based on solid-state reactions and manganese ions were incorporated into the structure of $SrSnO_3$. This was also confirmed at a temperature of 1,400°C. The sample prepared via the precipitation method formed a single-phase product at 1,050°C. At temperatures of 800°C and 950°C, the XRD results indicated a two-phase product, which could be described as $SrSnO_3$ and $SrMnO_3$. The formation of a multiphase product is caused by a generating strontium vacancy and the subsequent evaporation of SrO during crystal growth [41]. The next increasing calcination temperature resulted in the incorporation of manganese ions into the $SrSnO_3$ lattice and the production of a single-phase powder.

Table 1: Phase composition of the perovskite pigment of $SrSn_{0.9}Mn_{0.1}O_3$

Method	T [°C]	Detected phases
CCM	1050	$SrSnO_3$, SnO_2, Sr_2SnO_4
	1200	$SrSnO_3$
	1300	$SrSnO_3$
	1400	$SrSnO_3$
DMA	1050	$SrSnO_3$, SnO_2, $SrMnO_3$
	1200	$SrSnO_3$
	1300	$SrSnO_3$
	1400	$SrSnO_3$
WMA	1050	$SrSnO_3$, SnO_2, Sr_2SnO_4
	1200	$SrSnO_3$, SnO_2
	1300	$SrSnO_3$
	1400	$SrSnO_3$
PM	800	$SrSnO_3$, $SrMnO_3$
	950	$SrSnO_3$, $SrMnO_3$
	1050	$SrSnO_3$

Information regarding phase composition was also supplemented by obtaining XRD patterns at the chosen temperature of 1,200°C for all the solid-state reaction methods, and at 1,050°C for the PM (Figure 1). The main diffraction peak ($2\theta = 31.4$ °) for the WMA method was significantly shifted to the left, which was likely caused by the presence of the second phase (unreacted SnO_2). In addition, the results were supported by the lattice parameters and crystallite size (Halder-Wagner method) of the major phase of $SrSnO_3$, which crystallised in the orthorhombic structure (Table 2). The slight decrease of lattice parameters in all samples containing manganese ions ($SrSn_{0.9}Mn_{0.1}O_3$) indicated the successful incorporation of Mn ions into the

structure of $SrSnO_3$. These results are consistent with the size of the ionic radii, with substituted tin ions (Sn^{4+}, 0.069 nm, C.N=6) having a larger ionic radius than manganese ions (Mn^{4+}, 0.054 nm, C.N=6) [41].

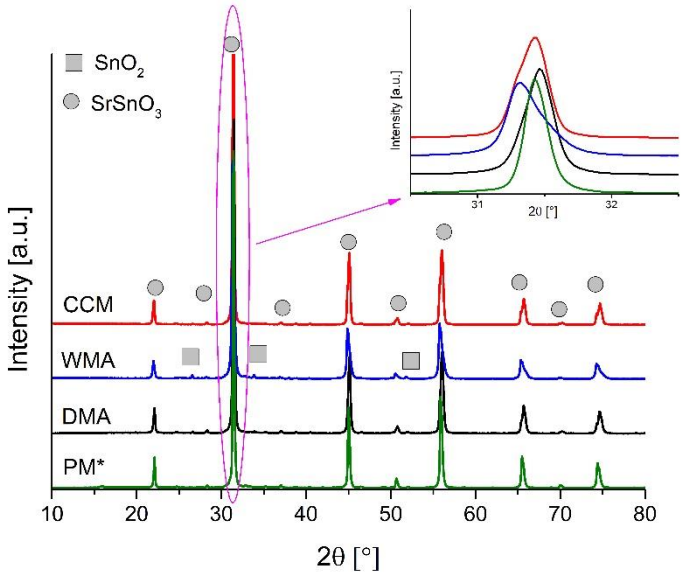

Figure 1: The XRD spectra of $SrSn_{0.9}Mn_{0.1}O_3$ prepared via different synthesis methods with a calcination temperature of 1,200°C for each and 1,050°C for the PM process

Table 2: Lattice parameters and crystallite size for the compounds $SrSn_{0.9}Mn_{0.1}O_3$ prepared using the different methods

Method	Detected phases	T [°C]	Lattice parameters [nm]			Crystallite size [nm]
			a	b	c	
PDF No. 01-081-2514	$SrSnO_3$	-	0.5708	0.8084	0.5711	-
CCM	$SrSn_{0.9}Mn_{0.1}O_3$	1200	0.5703	0.8025	0.5708	4.8
DMA		1200	0.5683	0.8068	0.5679	7.5
WMA		1200	0.5697	0.8057	0.5700	5.8
PM		1050	0.5705	0.8068	0.5705	7.6

3.2 Particle size distribution

This characteristic pertains to one of the most important properties of the pigment, which determines the appearance, gloss, colour properties and reflectance of any coatings. Therefore, it is of particular significance to measure and potentially adjust the grain size of the pigments. The results of the particle size distribution expressed by values of d_{50} and span are summarised in Table 3. The values of d_{50} of all the prepared pigments did not exceed a limit of 3.5 μm, with their values ranging from 1.0 to 3.5 μm. The increased values of d_{50} were recorded in the sample prepared via the DMA method. This was caused by the

more reactive surface from the mechanochemical activation process and the subsequent sintering of the powder during the calcination process. In this case, it would be suitable to extend the milling time, given that the recommended mean particle size distribution for an application of powder in the coating is approximately 2 μm [42]. The width of the pigment distribution curve ranged from 1.96 to 8.98. The higher values correspond to the lower calcination temperature (1,050°C for the solid-state reaction method), which relates to the results of the XRD analysis (many phases were detected at this temperature).

Table 3: Effect of the preparation method on the particle size distribution of the $SrSn_{0.9}Mn_{0.1}O_3$ pigment

Method	T [°C]	d_{50} [μm]	SPAN
CCM	1050	1.33	6.72
	1200	1.42	4.65
	1300	1.80	3.93
	1400	2.15	2.95
DMA	1050	1.38	4.08
	1200	2.18	3.92
	1300	2.96	3.34
	1400	3.51	3.60
WMA	1050	1.15	8.98
	1200	1.06	4.86
	1300	1.25	2.25
	1400	1.89	1.96
PM	800	1.91	3.86
	950	1.82	3.23
	1050	1.91	2.54

3.3 Morphological studies

Scanning electron microscopy (SEM) images of the calcined samples obtained via all the synthesis methods are shown in Figure 2. Here, it was clear that the sample prepared via CCM had various particles, with a small amount of spherical particles. The significance of the sintering process was confirmed by the micro-image of the DMA sample, indicating that it was caused by the superior reactivity of the particles due to the use of the dry mechanoactivation process. The agglomerates of the particles in the DMA sample exhibited irregular shapes, while the sample prepared via the WMA method had similarly shaped particles to the CCM sample. The PM method provided elongated particles with matchstick shapes, which was caused by the precursor and the lower calcining temperature.

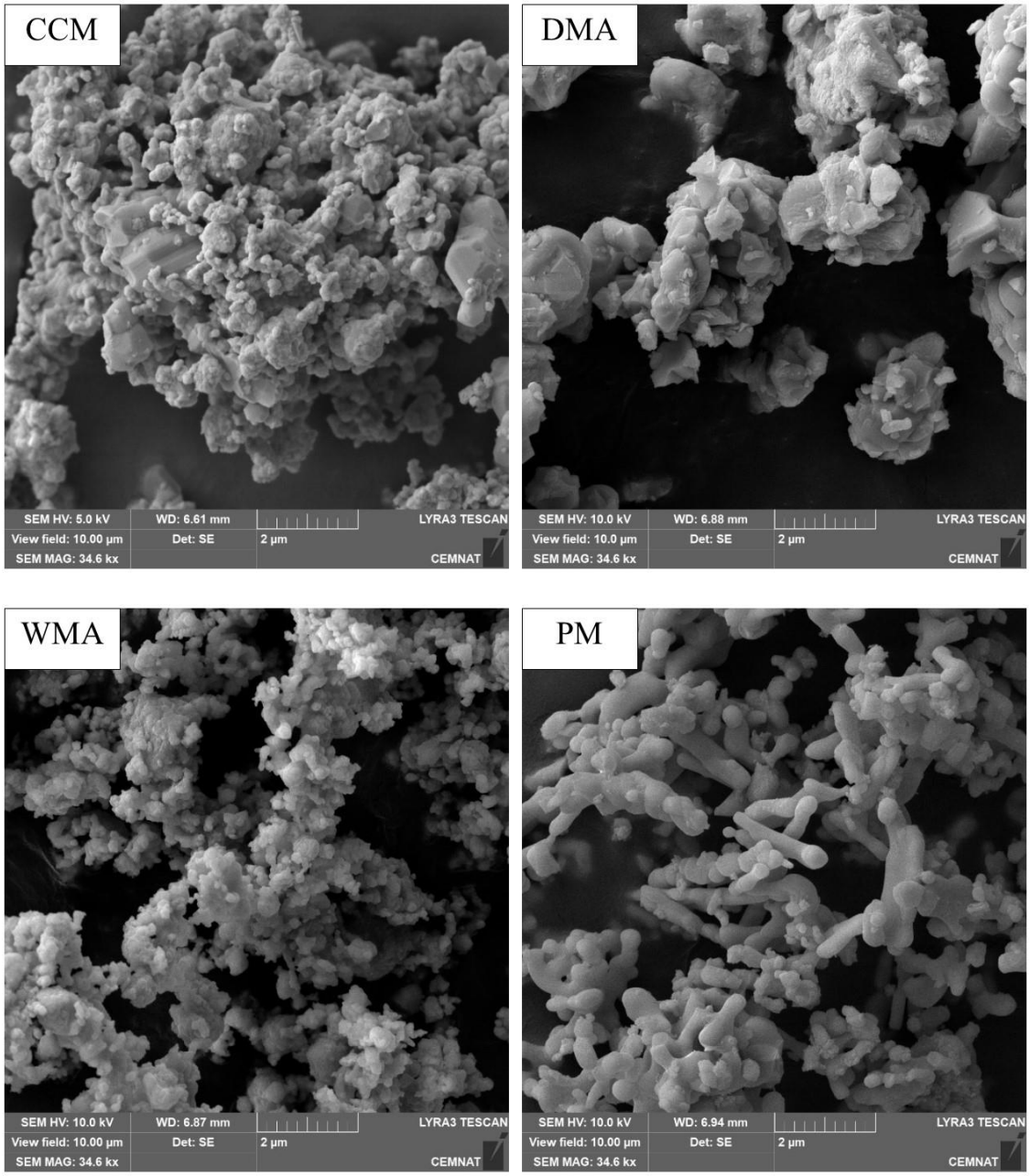

Figure 2: The SEM microphotographs of the perovskite samples prepared via the different methods at 1,200°C, and at 1,050°C for the PM process

3.4 Diffuse reflectance in the near-infrared region

The reflectance spectra and calculated solar irradiance ranged from 700 to 1,650 nm for the different synthesis methods at 1,200°C (solid-state reaction methods), at 1,050 °C (PM) and commercial Brown 10 pigment (Shepherd Color Company), as shown in Figure 3. The solar reflectance values are shown in Table 4. According to the ASTM G173-03 standard, the calculated values moved in the range of 24.7%–43.5%. Compared with the standard (R* = 30.5%), as pigments prepared by CCM, DMA at 1,050°C and 1,200°C,

WMA at 1,050°C and PM in the whole range of temperatures had higher solar reflectance data. At other calcining temperatures, the pigments had successively similar solar reflectance data as standard. Higher values were obtained in the samples prepared via the PM method, where lower calcining temperatures were used compared to in the solid-state reaction methods. However, all the preparation methods provided a pigment with a value of higher than 20% and could thus be considered as samples of a cool pigment [27]. Due to the high solar reflectance, the prepared samples are promising candidates for use as pigments in the colouring of roof and facade painting coats.

Table 4: Effect of the method of preparation on the calculated solar reflectance

Method	T [°C]	R* [%]
Brown 10	-	30.5
CCM	1050	39.8
	1200	40.2
	1300	34.2
	1400	31.9
DMA	1050	40.8
	1200	35.9
	1300	31.5
	1400	24.7
WMA	1050	39.7
	1200	31.4
	1300	32.8
	1400	31.0
PM	800	39.2
	950	43.5
	1050	42.0

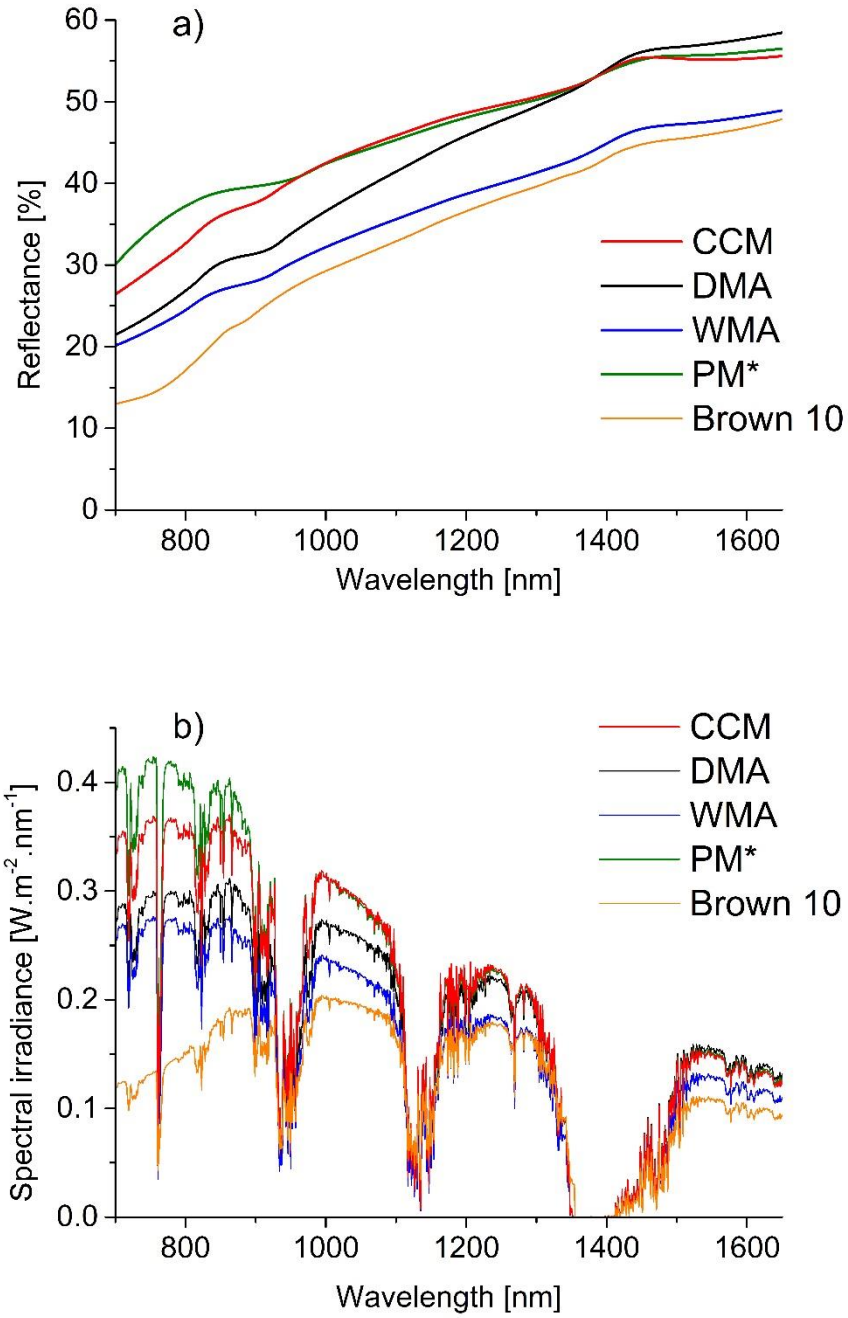

*Figure 3: Effect of preparation method on the (a) NIR reflectance and (b) solar irradiance of the calcined samples at a temperature of 1,200°C * and respectively 1,050°C*

3.5 Colour characteristics

The aim of this work was to study the influence of the preparation method and the calcination temperature on the colour properties of $SrSn_{0.9}Mn_{0.1}O_3$ pigments. As such, the colour characteristics of the powders and samples applied in the acrylic dispersion system were determined.

The colour properties of the powders ranged from peanut brown via dark-wood brown to café-noir brown hues in the case of the solid-state reactions. The PM method resulted in distinct brown hues, with the hue specifically shifting from tortilla brown to peanut brown. The measured colour coordinates of the pigments in powder form are summarised in Table 5. The results indicated that the colour coordinates of *L**, *a**, and *b** changed depending on the means of preparation and the heating temperature. The lightness *L** exhibited an irregular trend in the case of the CCM method and a range of interval of 44.3–59.9. Mechanochemical-activated pigments (DMA and WMA) with an increasing calcining temperature became darker because the values of *L** declined and shifted between 42.6 and 59.0. The negligible ascending trend of *L** with a growing temperature was observed in sample prepared via the PM method, with its values shifting in intervals from 56.6 to 58.9. All the pigments exhibited a red contribution of colour hue, which means that their values of *a** were positive and shifted in the range of 2.7–8.3. The CCM, DMA and WMA methods provided an alternate character of the coordinate *a**. The PM method exhibited an ascending trend of the *a** axis. The same trends as in the case of coordinate *a** also emerged in terms of coordinate *b**, with the high values of coordinate *b** also related to the high saturation of the samples and their values in the range of 8.9–18.4. In terms of the samples prepared via solid-state reactions in the range of 1,050°C–1,300°C, the chroma *C* had no specific character that was dependent on the calcining temperature, but their values rapidly declined at a temperature of 1,400°C, which was due to a drop in the colour coordinates of *a** and *b**. In terms of the PM method, the chroma *C* exhibited an ascending trend with the increase in temperature, which was largely related to the growth of the *b** coordinate (12.4→17.3). The chosen standard had a lower the contribution of yellow hue (*b**) than synthesised pigments. Therefore, the standard was a lower saturated (*C* = 8). Its colour shade can be compared to dark brown.

Table 5: The effect of preparation method on the colour properties of $SrSn_{0.9}Mn_{0.1}O_3$ powder

Method	T [°C]	L*	a*	b*	C
Brown 10	-	44.2	6.0	5.4	8.1
CCM	1050	59.9	4.4	15.4	16.0
	1200	51.4	7.2	15.7	17.3
	1300	53.3	7.7	15.9	17.7
	1400	44.3	6.6	9.6	11.6
DMA	1050	59.0	3.6	14.2	14.6
	1200	47.8	8.3	12.1	14.7
	1300	45.3	6.8	10.7	12.6
	1400	44.4	4.3	7.8	8.9

WMA	1050	58.6	2.7	11.9	12.2
	1200	47.4	5.6	10.7	12.1
	1300	45.7	8.3	10.3	13.2
	1400	42.6	7.5	7.5	10.6
PM	800	56.8	4.8	12.4	13.3
	950	57.5	5.4	14.2	15.2
	1050	58.9	6.3	17.3	18.4

The second colour characteristic was focused on the samples applied in the organic matrix (Table 6, Figure 4). In the samples prepared via the solid-state reaction methods, the coordinate L^* decreased with the ascending heating temperature, which caused the samples to become darker. In the case of the PM, the values of L^* exhibited a different character due to a dependence on the heating temperature, which meant the samples became lighter. The values of a^* had an irregular character with the increase in temperature in the samples prepared via solid-state reactions, with their values ranging from 4.3 to 6.9. When using the PM method, the values of a^* exhibited a growing trend with the increase in temperature, range between 3.9–6.1. The coordinates of b^* decreased with the increasing temperature in the sample prepared under dry conditions and reach values of 4.2 to 11.3. The PM method led to an increase in the value of b^* (8.4–11.4). The highest value of chroma C (12.9) was found out in the sample prepared via the PM method at 1,050°C.

When the pigments were applied to the organic binder, all the colour coordinates changed compared to the powder form. The highest change was observed in terms of the brightness of L^*, where there was a significant drop of 10–22. Therefore, the coating films appeared to have darker hues compared to the powder form. In the case of the colour coordinate a^*, there was a reduction in the contribution of the red hue following the application to the binder except in all samples prepared at 1,050°C. The red tint slightly increased at this temperature. In all the samples, there was a reduction in the contribution of the yellow tint following application to the binder, with a reduction of b^* in the range of 4–8. At the same time, the binder also reduced the chroma C of all the pigments. The resulting brown shade changed following application to the binder depending on the preparation method and the calcination temperature, from copper brown via chocolate brown to dark brown. The Brown 10 corresponded a chocolate brown hue. Unlike prepared pigments, the Brown 10 does not lose saturation C in the organic binder and its coordinate a^* and b^* negligible increased compared to the powder form.

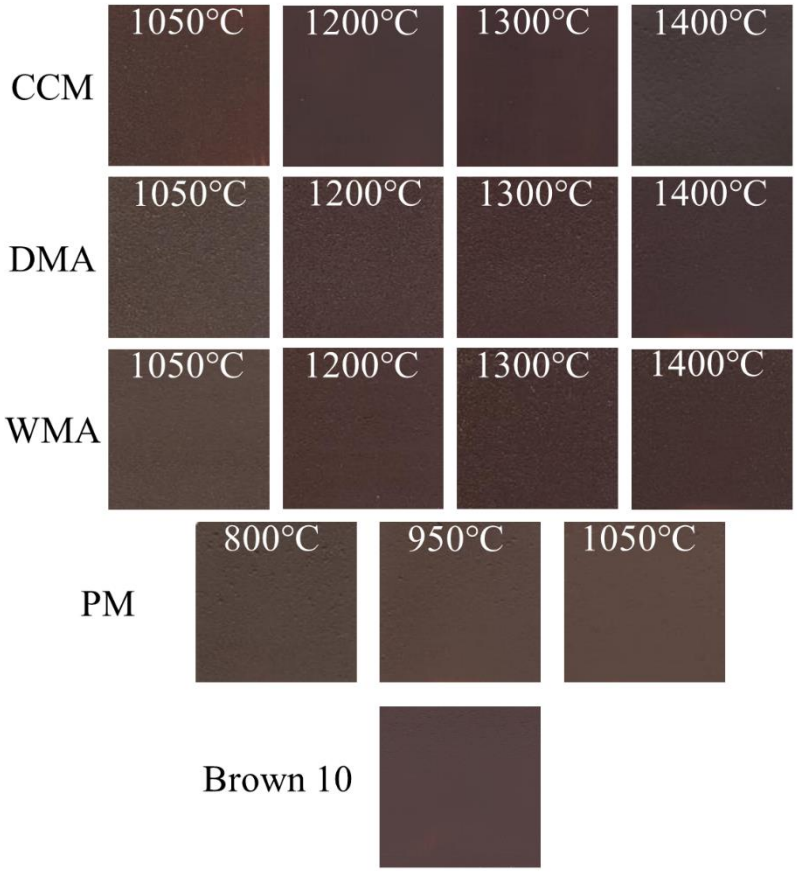

Figure 4: The colour possibilities of $SrSn_{0.9}Mn_{0.1}O_3$ applied in the organic binder

Table 6: The effect of the preparation method on the colour properties of $SrSn_{0.9}Mn_{0.1}O_3$ applied to the organic binder

Method	T [°C]	L*	a*	b*	C
Brown 10	-	31.5	7.3	5.6	9.2
CCM	1050	49.8	4.8	12.1	13.0
	1200	33.1	6.7	7.9	10.4
	1300	29.4	5.6	5.4	7.8
	1400	29.4	6.1	4.4	7.5
DMA	1050	37.6	4.3	10.1	11.0
	1200	31.7	6.9	7.6	10.3
	1300	31.3	6.0	6.8	9.1
	1400	31.0	4.8	5.6	7.4
WMA	1050	36.7	4.3	8.4	9.4
	1200	32.4	5.7	6.9	8.9
	1300	30.8	6.3	5.8	8.5
	1400	29.0	5.7	4.2	7.0
PM	800	36.0	3.9	8.4	9.3

	950	36.6	5.4	9.9	11.3
	1050	38.0	6.1	11.4	12.9

Based on the evaluation of the colour characteristics of both forms, the PM method and a temperature of 1,050°C are the best means for preparing a saturated brown colour, since the coordinates of chroma (C = 18.4 in powder form; respectively C = 12.9 in the paint coatings) and the coordinates of b^* (b^* = 17.3 in powder form; b^* = 11.4 in the paint coating) have higher values.

4 Conclusion

In summary, the NIR-reflective perovskite pigment, $SrSn_{0.9}Mn_{0.1}O_3$, was successfully synthesised via CCM, PM and the two mechanochemical activation methods. In the case of the PM, the single-phase orthorhombic Mn-doped $SrSnO_3$ was already obtained at 1,050°C, which represented a significant drop in calcined temperature compared to the solid-state reaction methods. The single-phase product was found at a temperature of 1,200°C in the samples prepared via CCM and DMA and at 1,300°C in the sample prepared via WMA. In terms of colour properties in a thin layer, the pigments exhibited a wide range of brown hues from copper brown via chocolate brown to dark brown. The mean of d_{50} was in the range of 1.0–3.5 μm and was dependent on the preparation method. Most samples met the required range of d_{50} (2 μm), which is a necessary condition for the pigments to be applicable in the organic binder. Higher values of d_{50} were achieved when using the DMA method, and it would be advisable to increase the milling time. The prepared pigments were characterised by a high solar reflectance in the range of 700–1,650 nm, with their values shifting in the range of 25%–44%, making them potential candidates for cool pigments. From an ecological and technological point of view, the PM approach is the most suitable method for the preparation of chocolate brown NIR pigments of $SrSn_{0.9}Mn_{0.1}O_3$.

Acknowledgement

This work was supported by the Grant Agency of Czech Republic (22-11397S) and the Ministry of Education, Youth and Sports of the Czech Republic (LM2023037). The authors thank the Centre of Materials and Nanotechnologies (CEMNAT) for the provision of UV-VIS-NIR spectroscopy.

Declaration of competing interest

The authors declare that they have no known competing financial interests or personal relationships that could have appeared to influence the work reported in this paper.

References

[1] S. Berri, N. Bouarissa, First-principle calculations to investigate structural, electronic, optical, thermodynamic, and thermoelectric properties of ABO_3 (A=Cs, Rb and B=Ta, Nb) compounds, Emergent Mater. 5 (2022) 1831-1847. https://doi.org/10.1007/s42247-021-00324-0.

[2] G. Mamba, P.J. Mafa, V. Mutharaj, A. Mashayekh-Salehi, S. Royer, T.I.T. Nkambule, S. Rtimi, 2022. Heterogenous advanced oxidation processes over stoichiometric ABO_3 perovskite nanostructures. Mater. Today Nano. 18, 100184. https://doi.org/10.1016/j.mtnano.2022.100184.

[3] H. Li, J. Yu, Y. Gong, N. Lin, Q. Yang, X. Zhang, Y. Wang, 2023. Perovskite catalysts with different dimensionalities for environmental and energy applications: A review. Sep. Purif. Technol. 307, 122716. https://doi.org/10.1016/j.seppur.2022.122716.

[4] Z. Yu, Ch. Deng, S. Kong, H. Hui, J. Guo, Q. Zhao, F. Tian, Ch. Zhou, Y. Zhang, S. Yang, H. Zeng, 2022. Transition metal-doped chalcogenide perovskite magnetic semiconductor $BaZrS_3$. J. Magn. Magn. Mater. 563, 169886. https://doi.org/10.1016/j.jmmm.2022.169886.

[5] X. Ye, Y. Wang, Z. Liu, B. Zhou, L. Zhou, H. Deng, Y. Long, Emergent physical properties of perovskite-type oxides prepared under high pressure, Dalton Trans. 51 (2022) 1745-1753. https://doi.org/10.1039/D1DT03551G.

[6] M. Vega, I.R. Martin, E. Cortés-Adasme, J. Llanos, 2022. Enhanced red up-conversion emission in Er^{3+}/Yb^{3+} co-doped $SrSnO_3$ for optical temperature sensing based on thermally and non-thermally coupled levels. J. Lumin. 244, 118687. https://doi.org/10.1016/j.jlumin.2021.118687.

[7] K.B. Bhojanaa, A.S. Mary, K.S. Shalini Devi, N. Pavithra, A. Pandikumar, 2022. Account of structural, theoretical, and photovoltaic properties of ABO_3 oxide perovskites photoanode-based dye-sensitized solar cells. Sol. RRL. 6, 2100792. https://doi.org/10.1002/solr.202100792.

[8] B. Mouhib, S. Dahbi, A. Douayar, N. Tahiri, O. El Bounagui, H. Ez-Zahraouy, 2022. Theoretical investigations of electronic structure and optical properties of S, Se or Te doped perovskite $ATiO_3$ (A=Ca, Ba, and Sr) materials for eco-friendly solar cells. Micro Nano. 163, 107124. https://doi.org/10.1016/j.spmi.2021.107124.

[9] P. Kumar, S. Singh, I. Gupta, V. Kumar, D. Singh, Luminous $LaAlO_3:Dy^{3+}$ perovskite nanomaterials: Synthesis, structural, and luminescence characteristics for white light-emitting diodes, Luminiscence. 37 (2022) 1932-1941. https://doi.org/10.1002/bio.4377.

[10] M. Hasan, S. Nasrin, M. Nazrul Islam, A.K.M. Akther Hossain, 2022. First-principles insights into the electronic, optical, mechanical, and theromodynamic properties of lead-free cubic ABO_3 [A=Ba, Ca, Sr; B=Ce, Ti, Zr] perovskites. AIP Adv. 12, 085327. https://doi.org/10.1063/5.0104191.

[11] I. Orak, A. Karabulut, E. Yigit, Ö. Sevgili, A. Rusen, F. Ozel, 2022. The diode and photodiode performances of $BaZrO_3$ perovskite-based device under the influence of thermal and light external stimuli. Sens. Actuator A Phys. 337, 113413. https://doi.org/10.1016/j.sna.2022.113413.

[12] Z.Y. Dai, Ch. Chen, G.S. Wang, Y.N. Lyu, N. Ma, Bandgap-tuned barium bismuth niobate double perovskite for self-powered photodetectors with a full-spectrum response, J. Mater. Chem. C. 11 (2023) 574-582. https://doi.org/10.1039/D2TC04310F.

[13] Q. Liu, F. Jin, B. Li, L. Geng, Structure and band gap energy of $CaSnO_3$ epitaxial films on $LaAlO_3$ substrate, J. Alloys Compd. 717 (2017) 55-61. https://doi.org/10.1016/j.jallcom.2017.05.112.

[14] A. Manoharan, M. Munusamy, A. Pradeep, S. Sellaiyan, S. Hussain, S. Krishnan, 2020. Effect of Pr doping on the optical and magnetic properties of calcium stannate perovskite nanostructures. Appl. Phys. A. 126, 874. https://doi.org/10.1007/s00339-020-04061-9.

[15] C.G. Pérez-Hernández, R. Sánchez-Zeferino, U. Salazar-Kuri, M.E. Álvarez-Ramos, 2021. Fabrication, structural properties, and tunable light emission of Sm^{3+}, Tb^{3+} co-doped $SrSnO_3$ perovskite nanoparticles. Chem. Phys. 551, 111324. https://doi.org/10.1016/j.chemphys.2021.111324.

[16] A. Marikutsa, M. Rumyantseva, A. Baranchikov, A. Gaskov, Nanocrystalline $BaSnO_3$ as an alternative gas sensor material: Surface reactivity and high sensitivity to SO_2, Mater. 8 (2015) 6437-6454. https://doi.org/10.3390/ma8095311.

[17] A. Kumar, B. Khan, V. Yadav, A. Dixit, U. Kumar, M.K. Singh, Rietveld refinement, optical, dielectric and ac conductivity studies of Ba-doped $SrSnO_3$, J. Mater. Sci.: Mater. Electron. 31 (2020) 16838-16848. https://doi.org/10.1007/s10854-020-04240-7.

[18] Q. Liu, F. Jin, G. Gao, W. Wang, Ta doped $SrSnO_3$ epitaxial films as transparent conductive oxide, J. Alloys Compd. 717 (2017) 62-68. https://doi.org/10.1016/j.jallcom.2017.05.080.

[19] Y. Liu, Y. Zhou, D. Jia, J. Zhao, B. Wang, Y. Cui, Q. Li, B. Liu, Composition dependent intrinsic defect structures in $ASnO_3$ (A=Ca, Sr, Ba), J. Mater. Sci. 42 (2020) 212-219. https://doi.org/10.1016/j.jmst.2019.10.015.

[20] F.Z. Salem, M.A. Ahmed, M.A. Sadek, M.G. Elmahgary, Novel hydrogen-doped $SrSnO_3$ perovskite with excellent optoelectronic properties as a potential photocatalyst for water splitting, Int. J. Hydrog. Energy. 47 (2022) 18321-18333. https://doi.org/10.1016/j.ijhydene.2022.04.055.

[21] K. Li, Q. Gao, L. Zhao, Q. Liu, 2020. Electrical and optical properties of Nb-doped $SrSnO_3$ epitaxial films deposited by pulsed laser deposition. Nanoscale Res. Lett. 15, 164. https://doi.org/10.1186/s11671-020-03390-1.

[22] H. Chen, N. Umezawa, 2014. Sensitization of perovskite strontium stannate $SrSnO_3$ towards visible-light absorption by doping. Int. J. Photoenergy. 2014, 643532. https://doi.org/10.1155/2014/643532.

[23] M.A. Riza, S. Sepeai, N.A. Ludin, M.A.M. Teridi, M.A. Ibrahim, Synthesis and characterization of $SrSnO_3$ using different synthesis methods, Malaysian J. Anal. Sci. 23 (2019) 100-108. https://doi.org/10.17576/mjas-2019-2301-12.

[24] Ž. Dohnalová, P. Bělina, N. Gorodylova, P. Šulcová, Green-coloured pigments with perovskite structure, J. Therm. Anal. Calorim. 125 (2016) 1233-1240. https://doi.org/10.1007/s10973-016-5464-0.

[25] Ž. Dohnalová, N. Gorodylova, P. Šulcová, M. Vlček, Synthesis and characterization of terbium-doped $SrSnO_3$ pigments, Ceram. Int. 40 (2014) 12637-12645. https://doi.org/10.1016/j.ceramint.2014.04.110.

[26] L. Adolfová, Ž. Dohnalová, P. Šulcová, New inorganic pigments based on $SrSnO_3$ doped by V_2O_5, J. Therm. Anal. Calorim. 113 (2013) 161-167. https://doi.org/10.1007/s10973-012-2931-0.

[27] Ž. Dohnalová, P. Šulcová, P. Bělina, Pink NIR pigment based on Cr-doped $SrSnO_3$, J. Therm. Anal. Calorim. 138 (2019) 4475-4484. https://doi.org/10.1007/s10973-019-08522-z.

[28] R. Oka, T. Masui, 2016. Synthesis and characterization of black pigments based on calcium manganese oxides for high near-infrared (NIR) reflectance. RSC Adv. 6, 90952. https://doi.org/10.1039/C6RA21443F.

[29] J. Zou, Z. Yu, Yellow β-Bi_2O_3/$BaCO_3$ complex pigments with impressive near infrared reflectance and excellent color performance, Sol. Energy Mater. Sol. Cells. 199 (2019) 99-107. https://doi.org/10.1016/j.solmat.2019.04.031.

[30] S. Sadeghi-Niaraki, B. Ghasemi, A. Habibolahz adeh, E. Ghasemi, M. Ghahari, Preparation of $(Fe,Cr)_2O_3$@TiO_2 cool pigments for energy saving applications, J. Alloys Compd. 779 (2019) 367-379. https://doi.org/10.1016/j.jallcom.2018.11.114.

[31] B. Kaur, N. Quazi, I. Ivanov, S.N. Bhattacharya, Near-infrared reflective properties of perylene derivatives, Dyes Pigm. 92 (2012) 1108-1113. https://doi.org/10.1016/j.dyepig.2011.06.011.

[32] S. Divya, S. Das, New red pigments based on Li_3AlMnO_5 for NIR reflective cool coatings, Ceram. Int. 47 (2021) 30381-30390. https://doi.org/10.1016/j.ceramint.2021.07.218.

[33] J. Zou, P. Zhang, Ni-doped $BaTi_5O_{11}$: New brilliant yellow pigment with high NIR reflectance as solar reflective fillers, Ceram. Int. 46 (2020) 3490-3497. https://doi.org/10.1016/j.ceramint.2019.10.063.

[34] W. Zhou, J. Ye, S. Zhuo, D. Yu, P. Fang, R. Peng, Y. Liu, W. Chen, 2022. Synthesis and characterization of novel yellow-green Al-doped $Y_3Fe_5O_{12}$ nano-pigments with high NIR reflectance. J. Alloys Compd. 896, 162883. https://doi.org/10.1016/j.jallcom.2021.162883.

[35] M. Fortuno-Morte, P. Serna-Gallén, H. Beltrán-Mir, E. Cordoncillo, The influence of Ca^{2+} and Zn^{2+} doping on the development of sustainable pigments based on $GdFeO_3$ perovskite: From a reddish colour towards a pure black, Ceram. Int. 48 (2022) 21428-21437. https://doi.org/10.1016/j.ceramint.2022.04.111.

[36] J. Hroch, Ž. Dohnalová, P. Šulcová, 2021. Study of reactions in the solid phase leading to the formation of $SrSn_{0.9}Mn_{0.1}O_3$ perovskite oxide. Thermochim. Acta. 706, 179054. https://doi.org/10.1016/j.tca.2021.179054.

[37] D. Yang, Ch. Zhang, L. Dong, X. Hou, W. Zheng, J. Xu, H. Ma, Synthesis and properties of $SrSn(OH)_6$ nanorods and their flame retardancy and smoke suppression effects on epoxy resin, J. Coat. Technol. Res. 16 (2019) 1715-1725. https://doi.org/10.1007/s11998-019-00254-x.

[38] K. Těšitelová, P. Šulcová, Synthesis and study of $Bi_2Ce_2O_7$ as inorganic pigment, J. Therm. Anal. Calorim. 125 (2016) 1047-1052. https://doi.org/10.1007/s10973-016-5322-0.

[39] ASTM G173-03, Standard tables for reference solar spectral irradiances: Direct normal and hemispherical on 37° tilted surface. https://doi.org/10.1520/G0173-03R20 , 2020 (accessed 14 July 2020).

[40] J. Luxová, K. Těšitelová, V. Podzemná, P. Šulcová, M. Bosacka, A. Blonska-Tabero, E. Filipek, 2019. Components of the $Co_3Cr_4(PO_4)_6$-$Cr(PO_3)_3$ system and the compound $CoCr_2(P_2O_7)_2$ as new ceramic pigments. Mater. Chem. Phys. 235, 121763. https://doi.org/10.1016/j.matchemphys.2019.121763.

[41] S.M. de Freitas, G.J.B. Júnior, R.D.S. Santos, M.V. dos S. Recende, 2019. Defects and dopant properties of $SrSnO_3$ compound: A computational study. Comput. Condens. Matter. 21, e00411. https://doi.org/10.1016/j.cocom.2019.e00411.

[42] G. Buxbaum, G. Pfaff, Industrial inorganic pigments, third ed., Wiley-VCH, Weinheim, 2005.